PHYSICAL REVIEW B VOLUME 51, NUMBER 8 15 FEBRUARY 1995-II

X-ray scattering from rotational disorder in epitaxial films: An unconventional mosaic crystal

P. F. Miceli
Department of Physics and Astronomy, University of Missouri–Columbia, Columbia, Missouri 65211

C. J. Palmstrøm*
Bellcore, Red Bank, New Jersey 07701
(Received 28 September 1994)

Motivated by x-ray-scattering measurements performed on ErAs(001)/GaAs(001) and $In_{0.7}Ga_{0.3}P(001)/GaAs(001)$, we present a model that explains the origin of a narrow peak and diffuse scattering, which are frequently observed at Bragg reflections in epitaxial systems. Central to the model is a correlation length for mosaiclike rotational disorder that arises in lattice-mismatched epitaxial films. The adhesive force between the film and the substrate is found to play a crucial role and leads to a striking anisotropy in the line shapes.

Throughout the history of crystal diffraction, the concept of a mosaic crystal, first proposed by Darwin,[1] has been both important as well as broadly applied to the interpretation of x-ray[2] and neutron[3] scattering from crystals with extended defects. Such an imperfect crystal is considered to contain many smaller crystals which have a slight misorientation with respect to one another. These "mosaic blocks" are large compared to the coherence length of the scattering experiment, so that the waves scatter without interference from different blocks. This rotational disorder causes Bragg peaks to broaden into arcs in reciprocal space with an angular peak width that is independent of the magnitude of the scattering vector—a distinguishing feature of mosaic line broadening. Such broadening can arise in real crystals from grain boundaries due to (spacially correlated) networks of dislocations which separate regions of defect-free crystallites. However, other extended defect configurations that introduce rotational disorder also exhibit this characteristic signature in the linewidths such as, for example, a random distribution of dislocations.[4] Moreover, most crystalline samples possess a variety of defects, so that mosaic line broadening is virtually unavoidable in practice unless one is dealing with a perfect crystal.

Despite the ubiquitous nature of mosaic crystals, there are several recent experimental results for metal[5–7] as well as semiconductor[8] epitaxial films containing misfit dislocations where the observed scattering cannot be interpreted using a conventional mosaic block model. In particular, there is a component of the line shape which is very narrow, implying long-range structural correlations. Yet it is known that disorder occurs on a much shorter length scale.[8] The purpose of this paper is to discuss the origin of these line shapes which now appear to be quite common in epitaxial films.

In this report the concept of a mosaic crystal is reconsidered as we address Bragg scattering from epitaxial systems with rotational disorder. A model is presented that introduces a correlation length for the rotational disorder, and it reduces to a conventional mosaic crystal in the limit of a long correlation length. Compared to bulk crystals, rotational disorder in epitaxial films tends to have a shorter correlation length, since reduced interfacial displacements are intrinsic to epitaxy. The importance of the substrate-film interfacial interaction is also apparent from the large anisotropy we observe in the rotational disorder. Two epitaxial systems are studied, ErAs(001)/GaAs(001) (Ref. 9) and $In_{0.7}Ga_{0.3}P(001)/GaAs(001)$, each having a 1.6% lattice mismatch with the substrate. The x-ray measurements used Mo $K\alpha_1$ radiation from a rotating anode and Ge(111) monochromator and analyzer crystals arranged nondispersively.

Figure 1(a) shows transverse scans across three Bragg positions located along the surface normal for an ErAs film 240 Å in thickness. The measurement geometry and scan direction in reciprocal space are shown in the insets to Figs. 1(b) and 2, respectively. A two-component line shape is observed at the (002) position; there is a sharp, resolution-limited ($<0.003°$) feature occurring at the specular condition ($Q_p=0$) as well as diffuse scattering which has a peak intensity an order of magnitude weaker. The sharp feature is not observed at higher-order Bragg reflections. These results do not depend on the azimuthal orientation of the sample. As shown in Fig. 1(b), the *angular* width of the diffuse scattering is independent of the scattering vector—a signature of disorder that is rotational in nature. However, these data cannot be explained in terms of a mosaic crystal, as it does not allow for the sharp feature at the (002).

The coexistence of Bragg (resolution-limited linewidth) and diffuse scattering is well known from the scattering theory for disordered crystalline solids, where the former component arises from long-range order and is attenuated by the uncorrelated disorder, whereas the latter component comes from the short-range correlations.[4] Examples include thermal vibrations and point defects in bulk crystals,[4] as well as roughness at surfaces.[10,11] Thus, an explanation of the present line shapes must include an analogous consideration of length scales for the displacements arising from rotational disorder. At short length scales the displacements are correlated and appear as

0163-1829/95/51(8)/5506(4)/$06.00 ©1995 The American Physical Society

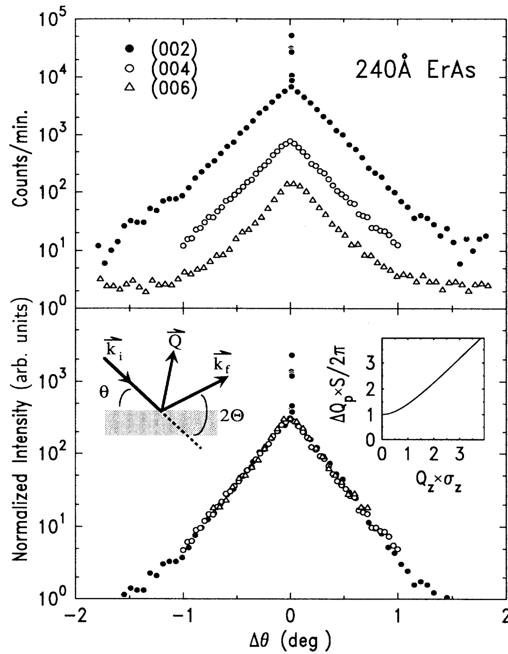

FIG. 1. (a) Transverse scans through specular Bragg reflections ($\Delta\theta \equiv \theta - \Theta$). Only (002) exhibits a resolution-limited component. (b) Same data renormalized: the angular width of the diffuse scattering is the same at all Bragg positions. One inset shows the scattering geometry, and the other inset is a plot of the diffuse scattering width, ΔQ_p, according to the model discussed in the text. Note that the angular peak width is $\Delta Q_p / Q_z$ and it approaches the mosacity ω as Q_z becomes large.

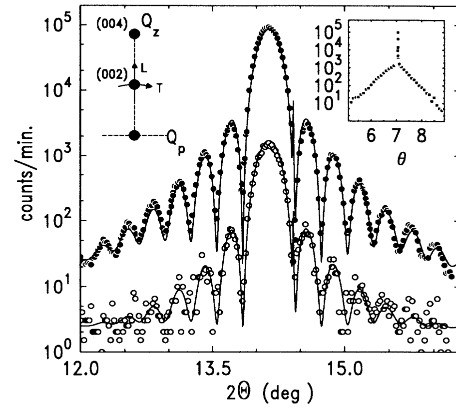

FIG. 2. Longitudinal scans at the (002) Bragg reflection of a 140-Å ErAs film showing interference fringes. Solid symbols: measured along the resolution-limited component (specular condition, $Q_p = 0$); open symbols: measured just off of the specular condition, at the peak of the diffuse scattering. The upper solid curve is obtained from fitting the specular data, and the lower solid curve is the upper curve multiplied by a constant factor. The direction of the longitudinal (L) and transverse (T) scans are shown in one inset, where Q_z is along the surface normal. The other inset shows a transverse scan along T.

simple rotations, producing the diffuse scattering in Fig. 1. At long length scales the displacements are uncorrelated but bounded in magnitude by the substrate. Therefore, the sharp component arises from a source of structural coherence not present in the mosaic crystal model, coming from the small displacements achievable in epitaxial systems.

It is of interest to build these ideas into a scattering model, and this is simplified by the data in Fig. 2 which locate the displacement fields. Longitudinal scans through the (002) Bragg reflection exhibit interference fringes due to the 140-Å ErAs thickness. There are two sets of data: one with the sample aligned at the specular condition, and the other where data were collected just off-specular, near the peak of the diffuse scattering. The curve is a least-squares fit to the specular data using a model described elsewhere,[12,13] and it indicates that a strain gradient along z can be neglected. After rescaling by a constant factor, the same curve also provides a good representation of the off-specular data, as shown, indicating[13,14] that the displacement fields begin at the film-substrate interface. Of course, this is exactly where one expects the displacements to originate, since they come from misfit dislocations which accommodate lattice mismatch at that interface.

The essential scattering features can be illustrated by a simple model where rotational disorder produces vertically uniform displacements $\mathbf{u}$ originating at the film-substrate interface. For the sake of clarity, interface roughness and scattering from the substrate are neglected, so that the differential scattering cross section for a thin film is given as

$$\frac{d\sigma}{d\Omega} = (2\pi n_A b)^2 A_{\mathrm{ir}} \frac{\sin^2(N_z Q_z c/2)}{\sin^2(Q_z c/2)} \times \left\{ e^{-\mathbf{Q}\cdot\underline{\sigma}^2(\infty)\cdot\mathbf{Q}} \delta(\mathbf{q}_p) + \frac{1}{(2\pi)^2} \int d^2\xi\, e^{i\mathbf{q}_p\cdot\xi} [e^{-\mathbf{Q}\cdot\underline{\sigma}^2(\xi)\cdot\mathbf{Q}} - e^{-\mathbf{Q}\cdot\underline{\sigma}^2(\infty)\cdot\mathbf{Q}}] \right\}, \tag{1}$$

where N_z is the number of lattice planes with spacing c, A_{ir} is the irradiated area, n_A is the number of atoms per area, and b is the scattering length. $\mathbf{Q}$ is the scattering vector with components Q_z and $\mathbf{Q}_p$ along the film normal and in the film plane, respectively, and $\mathbf{q}_p = \mathbf{Q}_p - \mathbf{G}_p$ where $\mathbf{G}_p$ is any reciprocal-lattice vector in the film plane. $2\sigma_{ij}^2(\xi) = \langle [u_i(\xi) - u_i(0)][u_j(\xi) - u_j(0)] \rangle$, with $i,j = x,y,z$ is the displacement-difference correlation function tensor which is assumed[11] to be a Gaussian random variable—an assumption addressed below. ξ is a rela-

tive coordinate for the atomic positions in the film plane, and the average $\langle\ \rangle$ is taken over all possible origins.

There are two multiplicative factors in this result, with the first giving the interference fringes observed in Fig. 2. The second factor is the transverse line shape which exhibits both resolution-limited and diffuse components. The δ function is multiplied by a Debye-Waller-like factor resulting from the root-mean-square (rms) displacements—it is responsible for attenuating the resolution-limited component with increasing scattering vector, as observed in Fig. 1(a).

We now examine the form of the displacement-difference correlation function that determines the transverse line shape. It can be constructed using a characteristic length S over which rotations of the crystal planes are correlated. Due to the nearly specular conditions in Fig. 1, where $\mathbf{G}_p=0$ and $Q\approx Q_z$, only the vertical displacements contribute, and we focus the discussion on the z component. At short length scales $\xi \ll S$, the displacements arise from rotations, so $\sigma_{zz}^2(\xi)=\omega^2\xi^2$, where ω is the rms rotation angle known as the mosaicity. At long length scales $\xi \gg S$, the uncorrelated displacements are bounded, giving $\sigma_{zz}^2(\infty)\approx\omega^2S^2$, which determines the attenuation of the resolution-limited component. These limiting values are conveniently restated in a scaling form often used to describe self-affine rough surfaces,[15] $\sigma_{zz}^2(\xi)=\sigma_{zz}^2(\infty)g_1(\xi/S)$, with $g_\alpha(x)=x^{2\alpha}$ if $x\ll 1$ and $g_\alpha(x)=1$ if $x\gg 1$ where, in the present case, $\alpha=1$ since the displacements are due to rotations.

The diffuse scattering integral in Eq. (1) is easily evaluated in two limits. When $e^{-Q_z^2\sigma_{zz}^2(\infty)}\ll 1$, the width of the diffuse scattering is $\Delta Q_p=\omega Q_z$, which means the angular width $\Delta Q_p/Q_z=\omega$ is independent of Q_z. This reflects the rotational character of the disorder. When $e^{-Q_z^2\sigma_{zz}^2(\infty)}\approx 1$, the width of the diffuse scattering is $\Delta Q_p=2\pi/S$ and is independent of Q_z, reflecting the finite correlation length of the rotational disorder. These results are summarized in the inset of Fig. 1(b).

Each of the three reflections in Fig. 1 satisfies the limiting case of weak specular scattering, $e^{-Q_z^2\sigma_{zz}^2(\infty)}\ll 1$. Correspondingly, and to a very high degree, the diffuse scattering exhibits an angular width $\Delta Q_p/Q_z$ that is independent of Q_z, as predicted by the model [high-Q_z limit in the inset to Fig. 1(b)]. We find[8] that thinner films exhibit stronger specular scattering due to their lower dislocation densities, and, thus, generally exhibit the other limiting case [low-Q_z limit in the inset to Fig. 1(b)], where ΔQ_p is constant with Q_z. This is illustrated by the data in Fig. 3 for a 72-Å-thick ErAs film which exhibits strong specular scattering, $e^{-Q_z^2\sigma_{zz}^2(\infty)}\approx 1$, for both the (002) and (006) reflections (when resolution is taken into account). The diffuse scattering width corresponds to a correlation length of ~ 100 Å. It is interesting that a recent study[7] of diffuse scattering in Nb/Al_2O_3 gives a similar correlation length. We speculate that diffuse scattering in both the ErAs and the Nb systems is just the independent scattering from individual dislocations. In summary, which limiting case is observed depends on the degree of disorder [i.e., the magnitude of $\sigma_{zz}^2(\infty)$].

Equation (1) predicts a Gaussian line shape for the diffuse scattering due to the assumption of a Gaussian random variable. This contrasts with the results observed in Fig. 1. However, one must distinguish between line shape and line width. Although the shape depends sensitively on the assumed statistical distribution function, the width is much more robust and depends only on the scaling arguments presented here. Thus, the width shown in the inset of Fig. 1(b) does not depend on this assumption. The approximation does, however, provide a convenient way to include rotational disorder simultaneously with self-affine rough interfaces in reflectivity models.

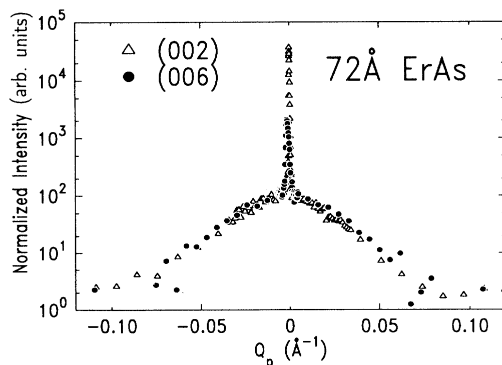

FIG. 3. Transverse scans through the specular Bragg reflections of a 72-Å-thick ErAs film. The in-plane momentum width ΔQ_p of the diffuse scattering is the same for both the (002) and (006) reflections.

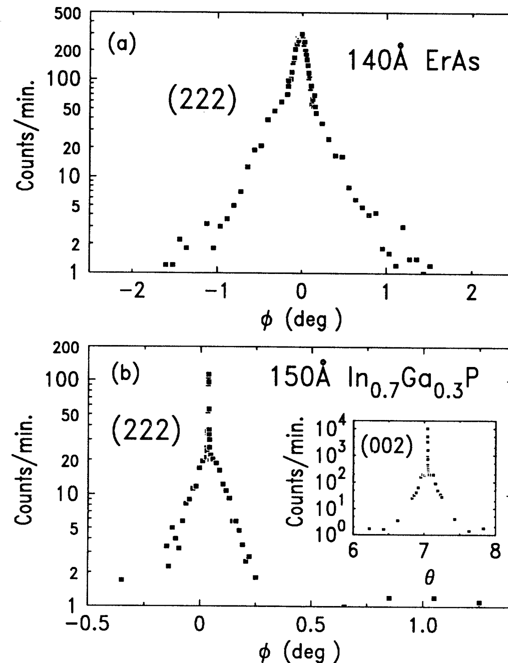

FIG. 4. (a) Scan through the (222) Bragg reflection along the azimuthal angle ϕ in the film plane for a 140-Å ErAs film. A resolution-limited component is not observed here nor on other samples of ErAs. (b) Same scan for 150 Å of $In_{0.7}Ga_{0.3}P/GaAs$, where a resolution-limited component is observed, in contrast to ErAs. The inset shows a transverse scan through the (002).

Although the near-specular conditions of Fig. 1 probe displacements perpendicular to the film plane, azimuthal rotations having displacement in the film plane are also anticipated. These may be observed by scanning the sample azimuthal angle ϕ through a Bragg reflection which has a component of the scattering vector in the film plane—such a scan is shown in Fig. 4(a) for the (222) reflection of the 140 Å ErAs film. This scattering is also described by Eq. (1). However, it is evident that a resolution-limited component is *not* present. Quite generally, for any film thickness, the resolution-limited component is never observed for these reflections, and the peak width simply increases with the dislocation density,[8] analogous to a conventional mosaic crystal. Therefore, $\sigma_{jj}^2(\infty)$ exhibits a pronounced anisotropy between the in-plane and out-of-plane directions: $\sigma_{xx}^2(\infty)=\sigma_{yy}^2(\infty) \gg \sigma_{zz}^2(\infty)$. In other words, the substrate is evidently less effective in organizing the film orientation in-plane than out-of-plane, suggesting that the adhesive force between the ErAs film and the GaAs is relatively weak. Indeed, the melting temperature of ErAs is ~2500 °C, indicating a large crystalline cohesive energy. Since GaAs has a much lower melting temperature, weak adhesion between ErAs and GaAs is likely.

To further explore the effect of adhesion on the observed line shapes, we investigated $In_{0.7}Ga_{0.3}P$/GaAs, where stronger adhesion is anticipated, since the cohesive and adhesive energies are comparable. The film thickness is 150 Å, and the composition was chosen so the lattice mismatch with GaAs is the same as for ErAs. The (002) reflection [inset Fig. 4(b)] is qualitatively similar to ErAs, but the (222) reflection, shown in Fig. 4(b), exhibits a resolution-limited component in striking contrast to any ErAs sample. Therefore, adhesion appears to be the essential factor explaining the differences between the two epitaxial systems. More importantly, this result demonstrates that the interaction of the film with the substrate plays a crucial role in determining the line shapes, with adhesion affecting the anisotropy.

In conclusion, we have considered Bragg reflections from epitaxial films using a simple model for rotational disorder. A more direct approach would calculate the scattering from some assumed configuration of misfit dislocations at the interface and we are currently pursuing this. Although such a calculation may provide more details (e.g., line shape), the present model captures the essential qualitative features in a simple manner: existence of Bragg and diffuse scattering due to rotational disorder, attenutation of the Bragg component, and the Q dependence of the diffuse scattering width. Therefore, our model is in the same spirit as the mosaic crystal model, and simplicity is achieved because the scattering process is sensitive to the length scales over which correlations change. In fact, for $S\rightarrow\infty$, our model is *identical* to a mosaic crystal, where the resolution-limited component is completely attenuated because the displacement fields are large.[16] Epitaxy limits the rms displacements, so a resolution-limited component can be observed.

Note added in proof. There is now evidence that Nb/Al_2O_2 exhibits the same delineation of scattering regimes as ErAs/GaAs. For 1500 Å of Nb, Reimer *et al.*[17] observe a mosaiclike Q dependence of the diffuse width, whereas Gibaud, McMorrow, and Swaddling[18] observe a correlation-limited Q dependence for 400 Å of Nb. Therefore, increasing the film thickness also increases σ^2 and this determines the scattering regime.

We thank S. K. Sinha, S. C. Moss, and H. Zabel for helpful discussions, and R. Bhat for the $In_xGa_{1-x}P$ sample. One of us (P.F.M.) gratefully acknowledges support from the University of Missouri Research Board.

*Present address: Dept. of Chemical Engineering and Material Science, University of Minnesota, Minneapolis, MN 55455.

[1] C. G. Darwin, Philos. Mag. **27**, 315 (1914); **27**, 675 (1914); **43**, 800 (1922).
[2] W. H. Zachariasen, *Theory of X-ray Diffraction in Crystals* (Dover, New York, 1967).
[3] G. E. Bacon, *Neutron Diffraction* (Oxford University Press, London, 1975).
[4] M. A. Krivoglaz, *Theory of X-ray and Thermal-Neutron Scattering by Real Crystals* (Plenum, New York, 1969).
[5] P. M. Reimer, H. Zabel, C. P. Flynn, and J. A. Dura, Phys. Rev. B **45**, 11 426 (1992); J. Cryst. Growth **127**, 643 (1993).
[6] A. Stierle, A. Abromeit, N. Metoki, and H. Zabel, J. Appl. Phys. **73**, 4808 (1993).
[7] A. Gibaud, R. A. Cowley, D. F. McMorrow, R. C. C. Ward, and M. R. Wells, Phys. Rev. B **48**, 14 463 (1993).
[8] P. F. Miceli, C. J. Palmstrøm, and K. W. Moyers, Appl. Phys. Lett. **58**, 1602 (1991).
[9] C. J. Palmstrøm, N. Tabatabaie, and S. J. Allen, Appl. Phys. Lett. **53**, 2608 (1988).
[10] S. R. Andrews and R. A. Cowley, J. Phys. C **18**, 6427 (1985).
[11] S. K. Sinha, E. B. Sirota, S. Garoff, and H. B. Stanley, Phys. Rev. B **38**, 2297 (1988).
[12] P. F. Miceli, C. J. Palmstrøm, and K. W. Moyers, Appl. Phys. Lett. **61**, 2060 (1992).
[13] P. F. Miceli, in *Semiconductor Interfaces, Microstructures, and Devices: Properties and Applications,* edited by Z. C. Feng (Institute of Physics, Bristol, 1993), p. 87.
[14] I. M. Tidswell, T. A. Rabedeau, P. S. Pershan, and S. D. Kosowsky, Phys. Rev. Lett. **66**, 2108 (1991); S. K. Sinha, Physica B **173**, 23 (1991).
[15] F. Family, Physica A **168**, 561 (1990).
[16] For sufficiently thick lattice-mismatched films where the substrate influence is small, conventional mosaic behavior is indeed observed. For example, see V. Hôly, J. Kubena, E. Abramof, K. Lischka, A. Pesek, and E. Koppensteiner, J. Appl. Phys. **74**, 1736 (1993).
[17] P. M. Reimer, H. Zabel, C. P. Flynn, and K. Ritley (unpublished).
[18] A. Gibaud, D. F. McMorrow, and P. P. Swaddling (unpublished).